SUPPLEMENTARY DATA

1. **Figure S1,** Related to Experimental Procedures: Electron Density at the Interface of the Dimer Spike

2. **Figure S2**, Related to Figure 1: Overlay of apo and +AT-130 Electron Densities

3. **Figure S3**, Related to Figure 2: The HBV Core Protein Homodimer

4. **Figure S4**, Related to Figure 4 and Experimental Procedures: Stereo Images of AT-130 Binding Sites, and AT-130 Isomers and *cis*-isomers of Related Phenylpropenamide Derivatives

5. **Figure S5**, Related to Figure 6: AT-130 in vivo Activity as Compared to HAPs

6. **Table S1, Related to Table 1:** +HAP1 and +AT-130 Unit Cell Comparison

7. **SUPPLEMENTARY EXPERIMENTAL PROCEDURES**

8. **Movie S1**, Related to Figure 3: Rigid-body movement of the A/B dimer

9. **Movie S2**, Related to Figure 3: Tertiary conformational changes of the C/D dimer

10. **Movie S3**, Related to Figure 4: Quasi-equivalent binding pockets with AT-130

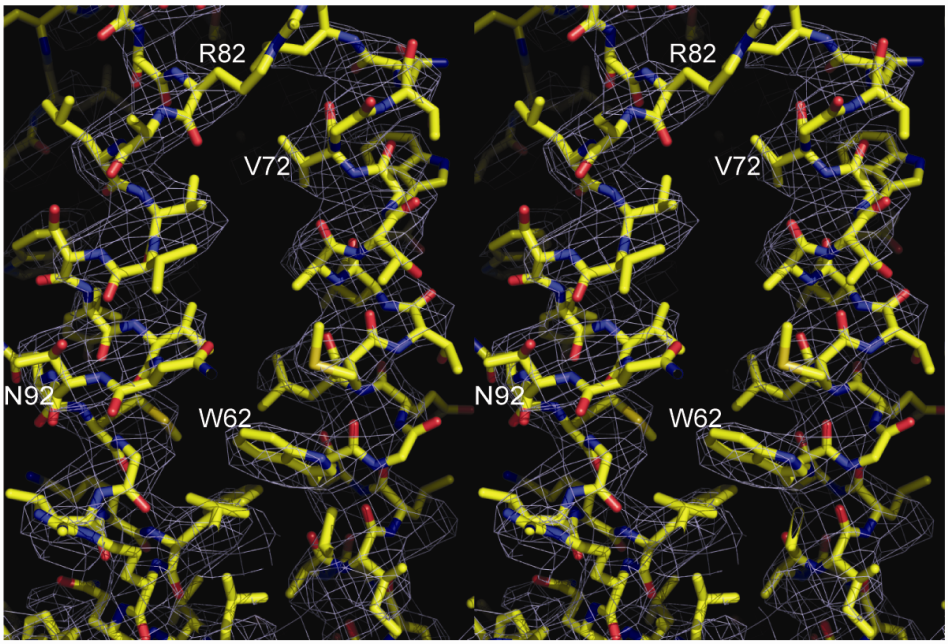

Figure S1, Related to Experimental Procedures: Electron Density at the Interface of the Dimer Spike

A stereo image of the typical B-sharpened density map (mesh) used for model rebuilding and refinement, shown here at the interface of the A/B dimer, with the refined model rebuilt into the density.

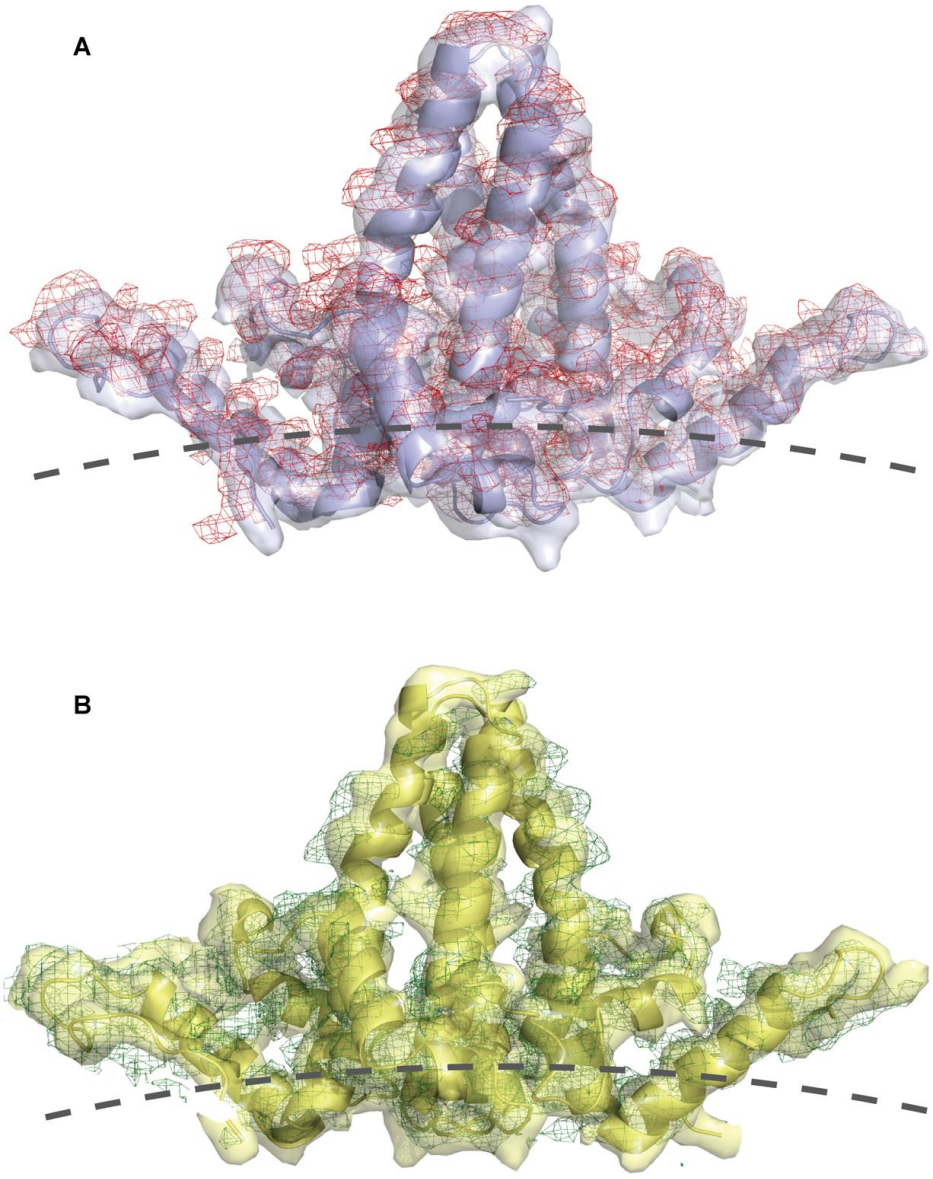

Figure S2, Related to Figure 1: Overlay of apo and +AT-130 Electron Density
(A) A/B dimer density mismatch. The 1QGT model structure shown as a blue ribbon, and the corresponding density as a blue surface. The +AT-130 2Fo-Fc density is shown as a red mesh (contoured at 1.5σ). The upward shift of the A/B subunit is most notable at the leftmost end of the A-monomer.
(B) C/D dimer density mismatch. The 1QGT model structure is shown as a yellow ribbon with corresponding density as a yellow surface. The +AT-130 2Fo-Fc density is the green mesh, showing little quaternary displacement but highlighting the outward bulging of the spike caused by AT-130. The dotted lines correspond to a capsid radius of 140Å.

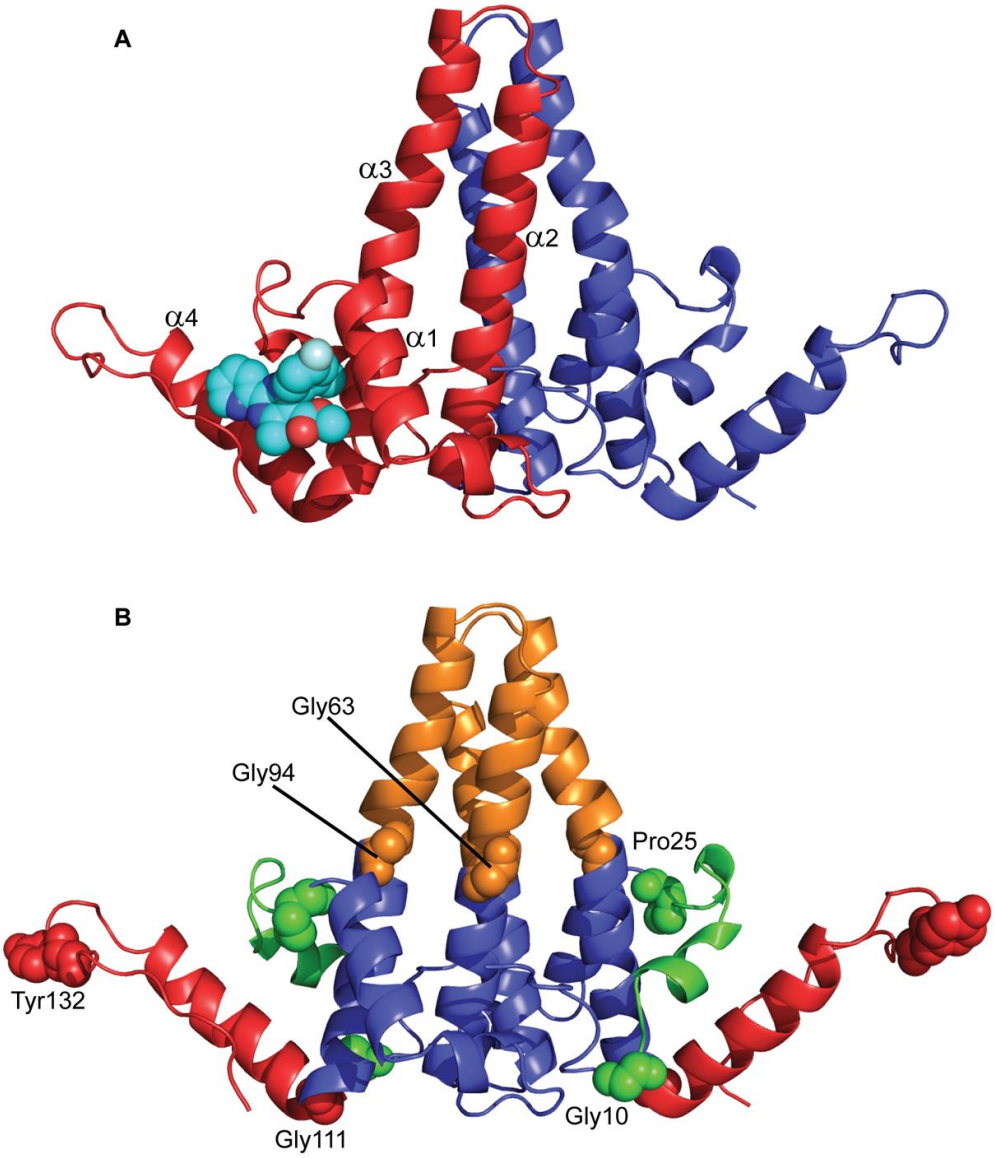

Figure S3, Related to Figure 2: The HBV Core Protein Homodimer

(A) The HBV core protein dimer has a largely α-helical structure. The four main helices are labeled as in Figure 2. HAP1 (cyan spheres) binds to a hydrophobic pocket located at the dimer-dimer interface.

(B) The domains of the HBV core protein. The four distinct domains are the central chassis domain (blue), the fulcrum helix (Gly10-Pro25, green), the spike tip (Gly63-Gly94, orange), and the contact domain (Gly111 to the C-terminus, including Y132, red). The glycines and proline (shown as spheres) delineate these domains and act as hinges, allowing each to move independently (Packianathan, 2010). In solution, free dimer has a more open configuration and adopts the more compact structure shown here upon assembly.

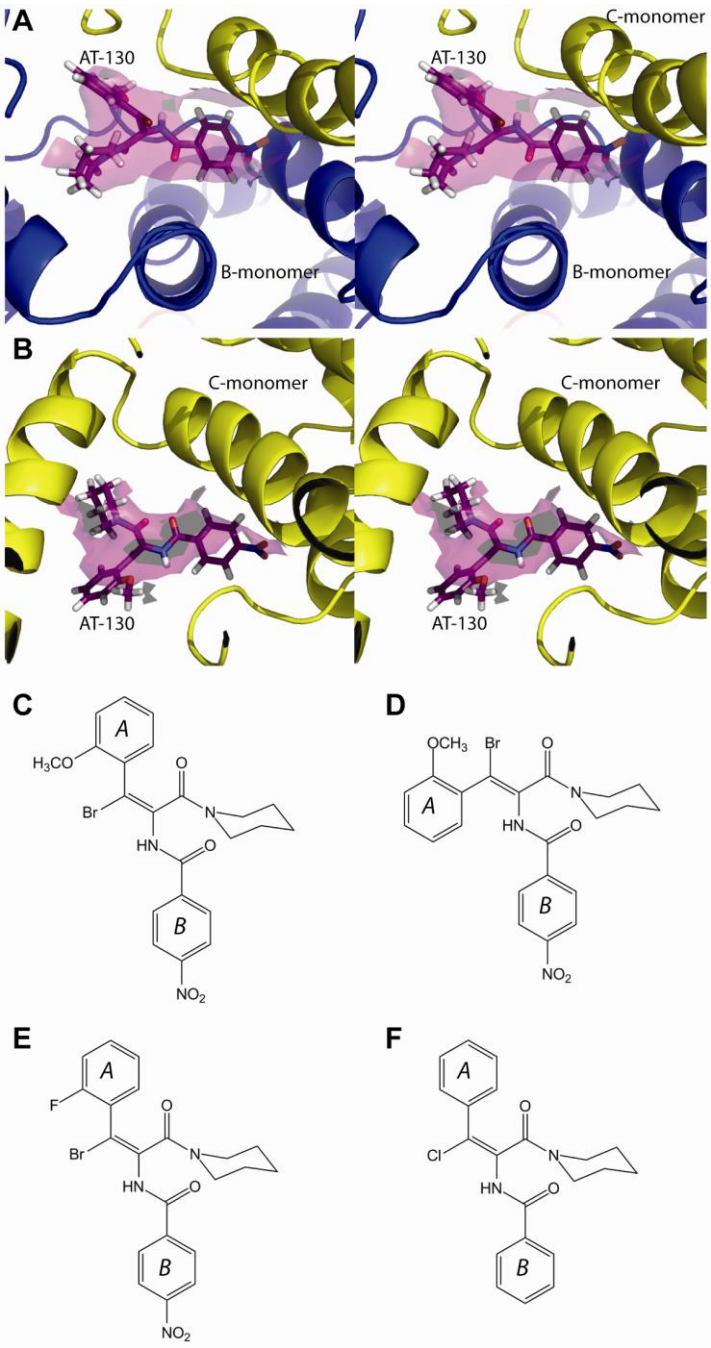

Figure S4, Related to Figure 4 and Experimental Procedures: Stereo Images of AT-130 Binding Sites, and AT-130 Isomers and *cis*-isomers of Related Phenylpropenamide Derivatives

(A) The B-pocket, with AT-130 density contoured to 2σ. (B) The C-pocket, with AT-130 density contoured to 1σ. (C) The *cis*-isomer of AT-130 around the vinyl bromide bond. (D) The *trans*-isomer of AT-130 around the vinyl bromide bond. (E) B-21 (Katen, 2010). (F) AT-61 (King et al., 1998). Density in panels A and B is sharpened with a B factor of -150.

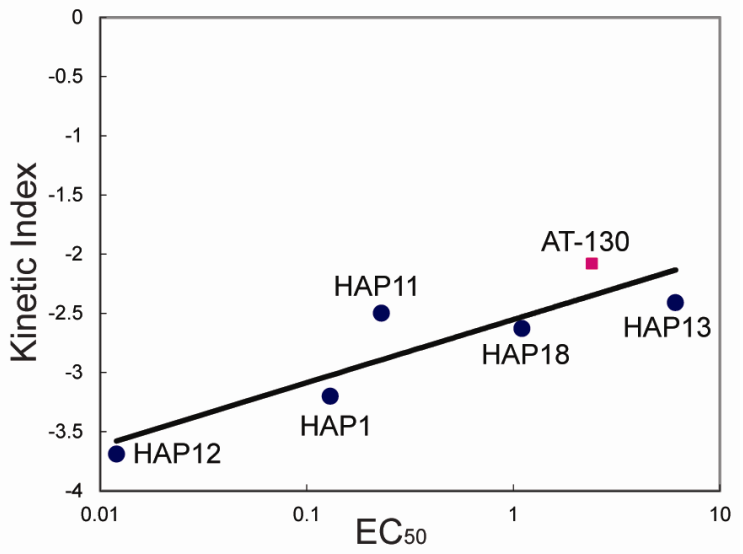

Figure S5, Related to Figure 6: AT-130 in vivo Activity as Compared to HAPs

AT-130 virus suppression properties correlate with the known HAP assembly effectors on the basic of kinetic effect alone.

Legends for movies

Movie S1, Related to Figure 3: Rigid-body movement of the A/B dimer
The A/B dimer from the apo 1QGT structure is morphed to the +AT-130 structure to show the upward motion of the dimer as a rigid body.

Movie S2, Related to Figure 3: **Tertiary conformational changes of the C/D dimer**
The C/D dimer from the apo 1QGT structure is morphed to the +AT-130 to show the tertiary structural changes at the spike tip.

Movie S3, Related to Figure 4: Quasi-equivalent binding pockets with AT-130
A display showing the icosahedral asymmetric unit and the unique quasi-equivalent binding sites. The AT-130-bound structure is shown as a ribbon diagram, with the electron density map contoured to 1.5σ shown as a gray solid. HAP1 (cyan) exclusively binds in the pocket at the base of the yellow C-monomer. Density is visible to 2σ, into which we were able to model the AT-130 (dark magenta) molecule. However, much stronger, clearer density is visible above 3σ in the blue B-monomer, into which we can clearly fit the *cis*-isomer of AT-130 (light magenta).

Table S1, Related to Table 1: +HAP1 and +AT-130 Unit Cell Comparison

Unit cell	Apo Cp149 (2G33)*	+HAP1 (2G34)*	+AT-130 (4G93)
a (Å)	558.4	528.5	527.4
b (Å)	327.1	366.6	362.8
c (Å)	562.2	540.1	538.2
β	109.1°	104.8°	105.1°

*from reference (Bourne et al., 2006)

SUPPLEMENTARY EXPERIMENTAL PROCEDURES

Sample Preparation Cp149 core protein (or capsid protein) dimer from Hepatitis B subtype *adyw* was expressed in E. coli from a pET11-based plasmid, pCp149. Cells were suspended in lysis buffer containing 50 mM Tris-HCl, pH 7.5, 100 mM NaCl, 5 mM DTT, 0.01 mg/mL DNase, 0.1 mg/mL RNase and cOmplete Protease Inhibitor Cocktail Tablets (Roche). Cells were lysed by sonication and centrifuged at 250,000xg for 30 minutes to remove cell debris. Solid $(NH4)_2SO_4$ was slowly added to the supernatant to a final concentration of 20% saturation. The solution was stirred for 1 h on ice, after which it was centrifuged at 25000xg for 1 h. The pellet was resuspended in ~50-60 mL of 100 mM Tris-HCl, pH 7.5, 100 mM NaCl, and 2 mM DTT (Buffer A) and loaded on a Sepharose CL-4B (GE Health Sciences) column equilibrated with column buffer A. HBV capsids were well separated from larger complexes and aggregates (which eluted in the void volume) and from soluble proteins of lower molecular weight. Fractions were then pooled on the basis of the chromatographic profile and SDS-PAGE, and then concentrated by ultrafiltration using a YM 100 ultrafiltration membrane (Amicon) to about 2.0 mg/mL. Concentrated protein was dialyzed against 50 mM sodium bicarbonate, pH 9.5, 1 mM DTT (Buffer N). Solid urea was added to 3.0 M and incubated on ice for 1.5 h. The now dissociated capsids were loaded onto a Sephacryl S-300 column (GE Health Sciences) equilibrated with Buffer N. Eluted fractions containing dimeric protein were pooled on the basis of SDS-PAGE analysis and concentrated by ultrafiltration using a YM 10 ultrafiltration membrane (Amicon) to about 2.0 mg/mL. Disassembled dimer was then dialyzed into 50mM Hepes, pH 7.5, and reassembled into capsids by the addition of NaCl to a final concentration of 0.5 M NaCl and incubated at room temperature for 2 h. Assembled capsids were purified from unassembled dimer and remaining small molecular weight contaminants by elution on a Sephacryl S-300 column equilibrated with Buffer N. Fractions containing purified capsids were again pooled on the basis of SDS-

PAGE analysis and concentrated by ultrafiltration using a YM 100 ultrafiltration membrane (Amicon) to about 2.0 mg/mL. The concentrated capsids were then again dissociated by dialysis against Buffer N, the addition of solid urea to 3.0 M, and incubation on ice for 1.5 h. The dissociated capsids were loaded onto a Sephacryl S-300 column equilibrated with Buffer N. Eluted fractions containing the purified, active dimeric capsid protein were pooled on the basis of SDS-PAGE analysis and concentrated by ultrafiltration using a YM 10 ultrafiltration membrane (Amicon) to about 2.0 mg/mL. Samples were passed through a 0.2 μm filter and stored at -80°C. Protein concentration was quantified by absorbance at 280 nm using an extinction coefficient of 60,900 $M^{-1}cm^{-1}$ (Zlotnick et al., 2002; Zlotnick, 1996). The V124W mutant was expressed and purified using a similar protocol, with the exception that reassembly was carried out at 50 mM NaCl and protein concentration was quantified with an extinction coefficient of 70,025 $M^{-1}cm^{-1}$ (Tan et al., 2013). Frozen aliquots of capsid protein were dialyzed against assembly buffer (50 mM Hepes, pH 7.5) prior to use in light scattering experiments.

For crystallization, a modified construct of wild-type Cp149 (3CA-Cp150) was used, wherein three native cysteine residues were mutated to alanine and an additional cysteine was appended at position 150; these mutations cause no structural changes compared to the native structure, improve the diffraction of resultant crystals, and stabilize capsids via inter-subunit disulfide crosslinking (Bourne et al., 2006). For crystallization, HBV capsids were expressed described above. Cells were lysed and RNA-filled capsids were precipitated and purified through the CL-4B size-exclusion step as described above. After CL-4B fractionation, RNA-filled capsids were pooled and T=4 3CA-Cp150 capsids were purified from free dimer and T=3 particles by sucrose gradient sedimentation. Sucrose solutions were mixed in 100 mM Tris-HCl, 100 mM NaCl; continuous 10-40% gradients were generated in SW28 tubes by tiled rotation using a Gradient Master (Biocomp). One mL capsid aliquots were layered on top of gradients

and centrifuged in an SW28 singing-bucket rotor (Beckman-Coulter) at for 4 hours at 28,000 RPM at 19°C. Bands were visualized by illumination and harvested via side puncture. Capsids were immediately dialyzed for crystallization into 5 mM Tris-HCl, pH 7.5, 150 mM NaCl. Dialyzed samples were first concentrated in a pressure concentrator (Amicon) to ~ 1 mg/mL, and then further concentrated to ~ 20 mg/mL in a spin concentrator (Vivaspin) (Bourne et al., 2006; Zlotnick, 1996; Zlotnick et al., 1999).

The phenylpropenamide compound *(E)-N-(1-bromo-1-(2-methoxyphenyl)-3-oxo-3-(piperidin-1-yl) prop-1-en-2-yl)-4*-nitrobenzamide (**AT-130**) was synthesized first from the generation of *(Z)-4-(2-methoxybenzylidene)-2-(4-nitrophenyl) oxazol-5(4H)-one (***2a***).* 4-Nitrohippuric acid (**1**, 0.5 g, 2.23 mmol) and *o*-anisaldehyde (0.276 g, 2.23 mmol), sodium acetate (0.183 g, 2.23 mmol) and acetic anhydride (0.6 mL) were combined and heated until the mixture just began to boil. It was transferred to an oil bath and heated just below the boiling point for 1 hour. Hot ethanol (2 mL) was added and the mixture was stirred until homogeneous and then cooled to room temperature. The resulting solid was collected by suction filtration and washed with a minimum quantity first of cold ethanol and then with boiling water (approx. 1 mL), and dried *in vacuo* to give **2a** (0.340 g, 68%). To a solution of oxazolone **2a** (0.5 g, 1.54 mmol) in chloroform at 0 °C, a solution of piperidine (0.129 g, 1.54 mmol) in chloroform (1 mL) was added dropwise. The yellow solution was stirred at 0 °C for 1 hour. Solid calcium carbonate (0.154 g, 1.54 mmol) was added, followed by dropwise addition of bromine (0.246 g, 1.54 mmol) in chloroform (2 mL). The resulting suspension was filtered to remove calcium salts, and the resulting solution was evaporated to dryness. The resulting orange oil was recrystallized from ethanol/water (4:1) to give compound **AT-130** (0.312 g, 67%) as a colorless powder (Katen, 2010).

Light Scattering Observation of kinetics by 90° light scattering was observed with a Photon Technology International fluorometer set to 400 nm for both excitation and emission (AT-130 absorbs significant amounts of light at 320nm) (Katen, 2010). Light scattering was measured for 10 µM (final concentration) wild-type Cp149 reduced with 5% β-mercaptoethanol; assembly was induced by addition of NaCl to a final concentration of 150 mM NaCl, with and without the addition of 20 µM AT-130. Reactions were performed using a black masked microcuvette with a 0.3 cm pathlength (Hellma) and incubated at 23˚C. The V124W assembly experiment followed the same procedure, with the exception that assembly was initiated with 50 mM NaCl due to the mutant assembly hyperactivity (data not shown). Light scattering is reported in arbitrary units. All experiments were repeated three or four times and the results averaged.

Electron Microscopy Samples from light scattering experiments were adsorbed to glow-discharged carbon over paralodian copper grids (EM sciences). Samples were stained with 2% uranyl acetate and visualized with a JEOL 1010 transmission electron microscope equipped with a 4Kx4K Gatan CCD camera.

Crystallization Crystallization was optimized from previously determined conditions for the *adyw* 3CA-Cp150 capsid in complex with the HAP compounds (Bourne et al., 2006). Co-crystals were grown with the addition of half-molar, equimolar, and twofold excess molar concentrations of AT-130 in DMSO (relative to the solution concentration of Cp in capsid form), followed by a 30min room temperature incubation prior to crystallization setup. Crystallization was carried out at room temperature with 4 µL sitting drops, initiated by a 1:1 mixture of protein solution with well solution. Protein solutions contained 10 mg/mL 3CA Cp150 capsid in 5 mM Tris buffer, pH 7.5, 150 mM NaCl, and 0.7-3% DMSO. Well solutions were composed of 5-10% polyethylene glycol 5000

monomethylether, 0-5% polyethylene glycol 8000 monomethylether, 6-28% 2,3-butanediol, 100 mM Tris pH 9.0, 150 mM NaCl, and 300 mM KCl. Crystallization of drug-free capsids is very slow, on the order of months. AT-130 increased nucleation and crystals typically appeared after 2-5 days, although diffraction-quality crystals were relatively rare.

Diffraction Data Collection Crystals were cryoprotected by gradually increasing the drop concentration of 2,3-butanediol to 20%. Cryoprotectant solutions maintained all other solution conditions, and contained 2 mg/ml uncrystallized capsid protein as a stabilizing agent, proven effective for cryoprotection of HAP1 co-crystals (Bourne et al., 2006). Crystals were flash-frozen in a stream of gaseous -170°C nitrogen. All crystals were screened in-house before transport to the Advanced Photon Source Beamlines 14BMC for data collection. The final dataset was collected from a single cryo-cooled crystal containing a 2:1 molar ratio of AT-130 to Cp dimer; crystallographic statistics are shown in Table 1.

Structure Solution and Refinement Molecular replacement and averaging was used for phasing. The native *adw*-like capsid 1QGT was used as the phasing model (Wynne et al., 1999). Molecular replacement was carried out with the Phaser program in the CCP4 program suite (McCoy, 2007). Phases calculated to 7 Å were subjected to 60-fold noncrystallographic symmetry (NCS) averaging and stepwise phase extension; phases were extended to 4.2 Å with 60-fold NCS averaging. Phases were extended by NCS averaging in one-lattice-step intervals with AVE by using masks calculated with MAMA, both from the RAVE suite (Kleywegt et al., 2001). NCS averaging produced an averaging R factor of 26.0% with a corresponding correlation coefficient of 93.7%. Output maps were calculated with SigmaA weighting in CCP4 (Collaborative Computational Project,

1994). B-sharpened maps were calculated using Fobs scaled by a negative Wilson B factor of -150. For the Fobs − Fcalc map, Fcalc included bulk solvent scaling, and one cycle of 60-fold NCS averaging was applied to the resulting map.

Refinement was carried out with CNS (Brunger et al., 1998) using strict icosahedral NCS, isotropic B-factor correction, and bulk solvent scaling. The E-monomer of the 2.25 Å *adyw* free dimer structure 3KXS was expanded into a complete asymmetric unit and used as the initial model. Necessary topology files for positional refinement of AT-130 were generated using the structural parameters of the Z-isomer of AT-61 (Figure S4F) (Wang, 2011). Bulk solvent scaling was adjusted by creating a protein mask of a defined radius. Refinement was carried out through positional refinement in conjunction with torsion molecular dynamics, with slow-cooling from 2,000 K in 50 K steps. Further positional refinement was iterated with 60-fold NCS averaging and manual rebuilding in Coot (Emsley, 2010). Three cycles of refinement were carried out, first using the averaged map as output by AVE, then re-refined using the B-sharpened map in order to favor geometrical constraints, and then a final round of refinement using the original averaged data (Supplementary Figure S6). For the final round, the geometry weighting factor (wa) was explicitly defined to favor geometric restraints given the low resolution. A test set of 5,000 reflections was flagged in thin shells and used for cross-validation, but the resulting R free was virtually unchanged from the crystallographic R factor due to NCS correlation of the test set with the refined data. The molecular model was refined to yield a crystallographic R factor of 37% (Table 1). This R factor values is consistent with those of other structures solved to comparable resolutions, such as the HK97 bacteriophage capsid which was solved to 3.45 Å with an R factor of 37.4% (Helgstrand et al., 2003), or the feline calcivirus capsid, which was solved to 3.4 Å with an R factor of 37.0% (Ossiboff, 2010).

Superpositions of models were carried out in Coot (Emsley, 2010), and generation of an apo map for Fcalc was done with Sfall from the CCP4 package using the 1QGT model in the appropriate unit cell and orientation from the Phaser solution (Collaborative Computational Project, 1994). Figures were generated from PyMol (DeLano, 2009) and Chimera (Pettersen EF, 2004).

REFERENCES

Bourne, C., Finn, M.G., and Zlotnick, A. (2006). Global structural changes in hepatitis B capsids induced by the assembly effector HAP1. J Virol *80*, 11055-11061.

Brunger, A.T., Adams, P.D., Clore, G.M., DeLano, W.L., Gros, P., Grosse-Kunstleve, R.W., Jiang, J.S., Kuszewski, J., Nilges, M., Pannu, N.S., *et al.* (1998). Crystallography & NMR system: A new software suite for macromolecular structure determination. Acta Crystallogr D Biol Crystallogr *54 (Pt 5)*, 905-921.

Collaborative Computational Project, N. (1994). The CCP4 Suite: Programs for Protein Crystallography. Acta Cryst D *50*, 760-763.

DeLano, W.L. (2009). The PyMOL molecular graphics system, version 1.21r1. Delano Scientific, San Carlos, CA.

Emsley, P., B. Lohkamp, W.G. Scott, and K. Cowtan (2010). Features and Development of Coot. Acta Cryst *66*, 486-501.

Helgstrand, C., Wikoff, W.R., Duda, R.L., Hendrix, R.W., Johnson, J.E., and Liljas, L. (2003). The Refined Structure of a Protein Catenane: The HK97 Bacteriophage Capsid at 3.44 A Resolution. J Mol Biol *334*, 885-899.

Katen, S.P., S.R. Chirapu, M.G. Finn, and A. Zlotnick (2010). Trapping of Hepatitus B Virus Capsid Assembly Intermediates by Phenylpropenamide Assembly Accelerators. Chem Biol *5*, 1125-1136.

King, R.W., Ladner, S.K., Miller, T.J., Zaifert, K., Perni, R.B., Conway, S.C., and Otto, M.J. (1998). Inhibition of human hepatitis B virus replication by AT-61, a phenylpropenamide derivative, alone and in combination with (-)beta-L-2',3'-dideoxy-3'-thiacytidine. Antimicrob Agents Chemother *42*, 3179-3186.

Kleywegt, G.J., Zou, J.Y., Kjeldgaard, M., and Jones, T.A. (2001). Around O. In International Tables for Crystallography, pp. 353-356, 366-367.

McCoy, A.J., R.W. Grosse-Kunstleve, P.D. Adams, M.D. Winn, L.C. Storoni, and R.J. Read (2007). Phaser Crystallographic Software. J Appl Crystallogr *40*, 658-674.

Ossiboff, R.J., Y. Zhou, P.J. Lightfoot, B.V. Prasad, J.S. Parker (2010). Conformational changes in the capsid of a calcivirus upon interaction with its functional receptor. J Virol *84*, 5550-5564.

Pettersen EF, G.T., Huang CC, Couch GS, Greenblatt DM, Meng EC, Ferrin TE. (2004). UCSF Chimera--a visualization system for exploratory research and analysis. J Comput Chem *25*, 1605-1612.

Tan, Z., Maguire, M.L., Loeb, D.D., and Zlotnick, A. (2013). Genetically altering the thermodynamics and kinetics of hepatitis B virus capsid assembly has profound effects on virus replication in cell culture. Journal of Virology *87*, 3208-3216.

Wang, P., Devan Nadhthambi, Ralph T. Mosley, Congrong Niu, Phillip A. Furman, Michael J. Otto, and Michael J. Sofia (2011). Phenylpropenamide derivatives: Anti-hepatitis B virus activity of the Z-isomer, SAR and the search for novel analogs. Bioorg Med Chem Lett *21*, 4642-4647.

Wynne, S.A., Crowther, R.A., and Leslie, A.G. (1999). The crystal structure of the human hepatitis B virus capsid. Mol Cell *3*, 771-780.

Zlotnick, A., Ceres, P., Singh, S., and Johnson, J.M. (2002). A small molecule inhibits and misdirects assembly of hepatitis B virus capsids. J Virol *76*, 4848–4854.

315 Zlotnick, A., Cheng, N., Conway, J.F., Booy, F.P., Steven, A.C., Stahl, S.J., and
316 Wingfield, P.T. (1996). Dimorphism of Hepatitis B Virus Capsids Is Strongly Influenced
317 by the C-Terminus of the Capsid Protein. Biochemistry *35*, 7412-7421.
318 Zlotnick, A., Palmer, I., Stahl, S.J., Steven, A.C., and Wingfield, P.T. (1999). Separation
319 and Crystallization of T=3 and T=4 Icosahedral Complexes of the Hepatitis B Virus Core
320 Protein. Acta Cryst D *55*, 717-720.
321
322